Mineralium Deposita (2004) 39: 301–312
DOI 10.1007/s00126-003-0403-y

ARTICLE

**Gilles Levresse · Eduardo González-Partida
Alejandro Carrillo-Chavez · Jordi Tritlla
Antoni Camprubí · Alain Cheilletz · Dominique Gasquet
Etienne Deloule**

Petrology, U/Pb dating and (C-O) stable isotope constraints on the source and evolution of the adakite-related Mezcala Fe-Au skarn district, Guerrero, Mexico

Received: 5 September 2003 / Accepted: 4 December 2003 / Published online: 3 March 2004

Abstract The Mezcala gold district, Guerrero, Mexico, is a Cretaceous to early Paleocene oxidized Fe-Au skarn deposit, genetically associated with an adakitic magmatic event of 63 ± 2 Ma, dated by ion-probe U/Pb on zircons.

The inner and outer alteration patterns and the mineralogical sequence (high garnet/pyroxene ratio, high ferric/ferrous ratio > 1, predominance of Fe-poor garnet and pyroxene, low total sulfides) found in Mezcala are compatible with the description of an oxidized gold skarn type. Carbon and oxygen isotope analyses of the inner calcite zone (−9.98 to −11.64 and +13.21 to +14.59‰, respectively) unequivocally support a magmatic signature of the hydrothermal fluid. Carbon and oxygen isotopes from the outer calcite zone (−8.81 to +3.45 and +12.95 to +22.77‰, respectively) suggest a complex mechanism of degassing and subsequent cooling/dilution of the resulting magmatic brine with the meteoric water. Gold appears to be closely associated with the adakite stock, whereas its transport is related with the outflow of highly oxidized magmatic brines from the intrusion. The gold precipitation is triggered by cooling/dilution of the degassed magmatic brine by the meteoric fluids.

Keywords Fe-Au skarn · C-O stable isotope · U/Pb dating · Paleocene · Mexico

Editorial handling: D. Lentz

G. Levresse (✉) · E. González-Partida · A. Carrillo-Chavez
J. Tritlla · A. Camprubí
Programa de Geofluidos,
Centro de Geociencias UNAM-Campus Juriquilla,
AP 1–253, 76230 Querétaro, México
E-mail: glevresse@geociencias.unam.mx
Tel.: +52-44-22381116
Fax: +52-44-22381100

A. Cheilletz · D. Gasquet · E. Deloule
Centre de Recherches Pétrographiques et Géochimiques,
CRPG-CNRS and Ecole Nationale Supérieure de Géologie,
BP 20, 54501 Vandoeuvre-les-Nancy, France

Introduction

The Mezcala Fe-Au district (Fig. 1) is made up by three main deposits: (1) Agüita/Filos, (2) Bermejal and (3) Nukay (Fig. 2). Current identified resources in the entire district are estimated to be around 2,000,000 oz Au. This study provides new data on the alteration minerals and their compositions, U/Pb dating of zircons, and carbon and oxygen isotopic compositions on carbonates in order to elucidate the origin of the ore-forming fluids and the geologic evolution of the Mezcala skarn deposits.

Adakite magmas belong to the calc-alkaline suite and have characteristic geochemical signatures that suggest that these melts originated by partial melting of subducting oceanic crust (Defant and Drummond 1990; Maury et al. 1996). Previous geochemical studies on Mezcala (González-Partida et al. 2003) revealed both the adakitic character of these granodioritic intrusions and the high oxidation state of the magmas during emplacement.

De la Garza et al. (1996) described both the geology of the Bermejal area and the preliminary skarn petrology. More recently, detailed petrographic and fluid inclusion work on these deposits (Jones and Jackson 2001; González-Partida et al. 2003; Levresse and González-Partida 2003) revealed a prograde and retrograde evolution of the alteration system (Table 1).

Contact skarn formation at the Mezcala Fe-Au deposits occurred between the Morelos Formation and an adakite stock. N–S and WNW–ESE fault intersection acted as the main channelway for both stock emplacement and fluid flow. The deep source of the pluton is supported by its adakite character, whereas the highly oxidized character is established by the presence of hematite trapped in the late magmatic fluid inclusions in quartz. The fluids associated with both prograde skarn formation and mineralization were high-temperature NaCl-KCl-bearing brines (Table 1). The high tempera-

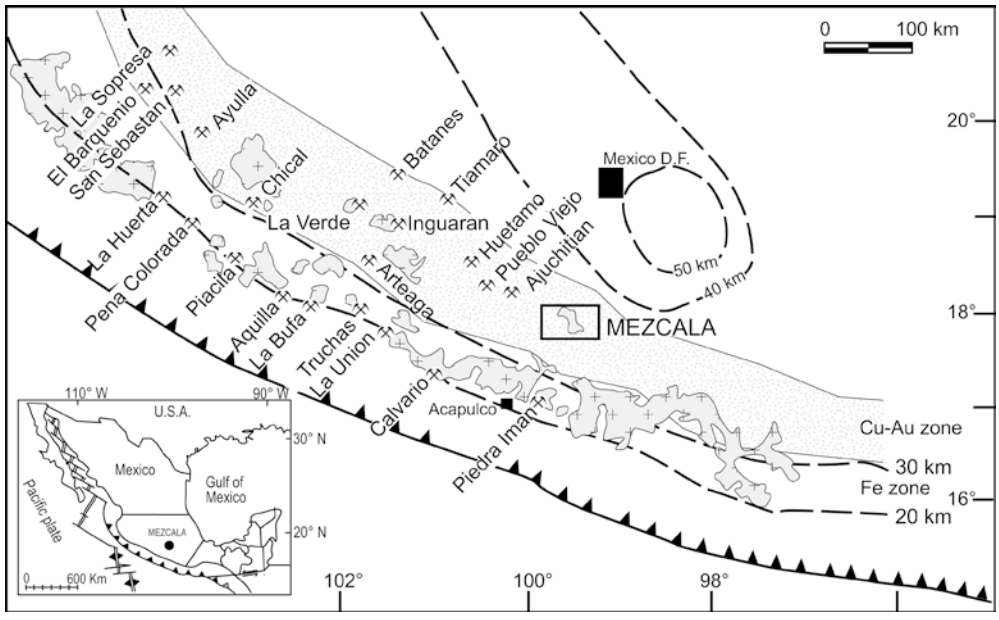

Fig. 1 Location map of Mezcala mining district and the Fe and Fe-Au metallic belt of the Sierra Madre del Sur, south-central Mexico. *Dashed lines* indicate crustal thickness

ture and salinity evolution documented in the Mezcala Fe-Au skarn deposit (González-Partida et al. 2003) is consistent with the systematic association of igneous rocks with gold mineralization (Hedenquist 1987; Sillitoe 1988; Meinert 1992; 1995; Meinert et al. 1997). The fluids associated with the retrograde alteration have lower temperatures and salinities (Table 1).

Geological setting

The Mezcala Fe-Au skarn district is located in the central part of the Guerrero state, halfway between Mexico City and Acapulco. It belongs to a mineralized belt containing porphyry copper deposits, epithermal deposits, Fe-Au-bearing skarn deposits and recently reported IOCG deposits (Tritlla et al. 2003) (Fig. 1). According to Clark et al. (1982), most of the Cu-Au deposits in Mexico and southwest USA were formed during the Laramide Orogeny. The Cu-Au, Fe-Au and polymetallic belts from the west-central part of Mexico are related with the lateral migration of the continental magmatic activity during late Cretaceous and early Tertiary times (González-Partida and Torres-Rodriguez 1988).

The studied area is located within the Balsas-Mezcala basin, which is part of the physiographic and magmatic "Sierra Madre del Sur" (SMS) province. The rocks in the SMS range from early Paleocene to Miocene, and form a wide calc-alkaline magmatic province (Morán-Zenteno et al. 1999). These authors suggested that the SMS was developed after the Laramide Orogeny (post-collision zone) in a fast convergent, thick continental crust subduction regime.

The Mezcala adakite stocks intruded a Cretaceous calcareous and argillaceous sedimentary sequence (Morelos, Cuautla and Mezcala formations; Fríes 1960) with a thickness of more than 2,000 m (Fig. 2A–B). The Albian-Cenomanian Morelos Formation is made up by alternating limestone and dolostone beds, with some flint nodules horizons, and silicified fossil fragments. Locally, a pure anhydrite member crops out at the base of this formation. An explosive volcanic rock of Oligocene age crosscuts and overlies all the formations. This sedimentary sequence was deformed during the Laramide Orogeny.

Gold mineralization at Mezcala occurs both in Fe-Au skarns developed along the margins of the stocks and disseminated within the hydrothermal potassic (orthoclase, scapolite, antigorite) alteration area of the intrusives (Fig. 2). The mineralization consists of pervasive botryoidal and massive hematite with disseminated gold (De la Garza et al. 1996).

Skarn characteristics: alteration and mineralization

Alteration and mineralization relationships were examined by mapping, petrography and electron microprobe analyses. Mineral composition and paragenesis and its relationship with the alteration events are shown in Figs. 3 and 4. Mineral phases and compositions were determined using a Cameca SX 100 electron microprobe at the UHP University of Nancy, France (Table 2).

Gold mineralization at Mezcala always occurs in skarn rocks developed vertically along the margins of adakite stocks, preferentially at the WNW–ESE margins (Jones and Jackson 2001). Endoskarns are usually poorly developed whereas exoskarns, formed within regional limestones, can attain up to 100 m in thickness. The hydrothermal alteration is controlled by N–S and WNW–ESE faults, bedding planes and reactive rocks of the Morelos Formation. According to previous data (González-Partida et al. 2003; Levresse and González-

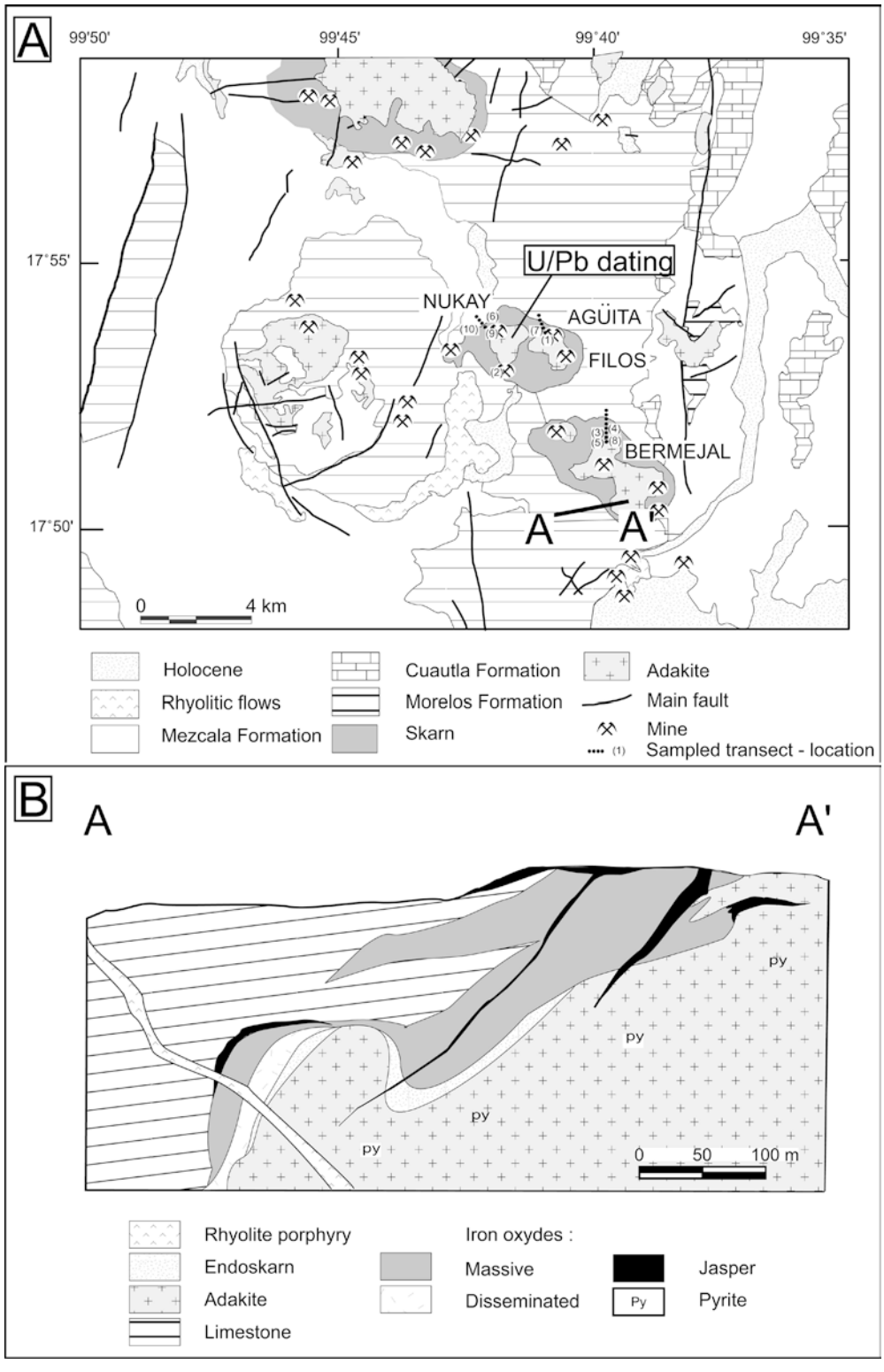

Fig. 2 *A* Geological map of the area hosting the Mezcala Fe-Au skarn deposits; **B** Simplified geological cross-section drawn for the A-A' transect. U/Pb dating: localization of the drill core used for U/Pb zircon dating. Sample transect: samples used for petrography, fluids inclusion and C-O isotopic studies

Partida 2003), the skarn represents a prograde phase controlled by magmatic-dominated fluids whereas the retrograde phase probably involves significant amounts of meteoric fluids (Fig. 3a).

The prograde phase is characterized by the development of both the endoskarn and the exoskarn. The endoskarn typically consists on a metasomatic zoning inwards from the adakite margin made up by (1) garnet (Gr and Ad) > pyroxene (Di to Hd), (2) pyroxene > garnet and (3) pyroxene (Fig. 4). Individual pyroxene and garnet crystals typically are 0.1 to 1 cm in diameter and range up to 10 cm. The earliest pyroxene assem-

Table 1 Summary of fluid inclusion data (González-Partida et al.2003) and stable isotope results of the ore-bearing skarn, the retrograde alteration and the unaltered limestone of the Mezcala Fe-Au skarn deposits (this study)

Sample	Host	N	Th range	Th average	Tf NaCl/Tmi range	Tf NaCl/Tmi average	Salinity wt% NaCl	Wt% NaCl average	N	$\delta^{13}C_{VPDB}$ (in per mil)	$\delta^{18}O_{VSMOW}$ (in per mil)
Late-magmatic alteration											
Aguita	Qz	48	290 to 515	400	320 to 513	371	40 to 55.5	44.5			
Bermejal	Qz	26	355 to 700	492	268 to 388	319	26	35 to 45			
Filos	Qz	108	358 to 635	393	197 to 510	383	30.5 to 57	44			
Inner alteration zone											
Aguita	Qz	55	317 to 514	363	−3.5 to −10	−7	5.7 to 13.9	9			
Filos	Qz	79	218 to 410	273	−13.5 to −20.1	−17.3	16.9 to 22.4	20.9			
	Qz	32	165 to 389	268	235 to 415	329	30 to 50	39			
Nukay	Qz	142	122 to 510	290	177 to 507	341	28 to 56.5	41			
Bermejal	Qz	105	200 to 388	288	200 to 399	300	31 to 45	38.5			
	Qz	15	325 to 568	398	−20 to −21	−20.5	15	22.3 to 23			
	Ca	46	238 to 360	276	225 to 340	277	23	31 to 40	15	−9.98 to −11.64	+13.21 to +14.59
Outer alteration zone											
Bermejal	Qz	40	290 to 338	320	230 to 347	266	40	33 to 34			
	Qz	100	123 to 340	234	−17.8 to −1.9	−8.8	3.2 to 35	9			
	Ca	22	190 to 242	211	232 to 246	237	33 to 33.3	33.1			
	Ca	66	152 to 282	219	−11.5 to −1.6	−3.5	−1.7 to 15.5	5.4			
Filos	Qz	265	127 to 340	247	−19.5 to −1.1	−8.1	10.3	10.9			
Nukay	Qz	114	151 to 297	191.4	−15.7 to −3.4	−9.7	19.2 to 5.4	13.2			
	Ca	30	135 to 155	144	−7.2 to −7.2	−7.2	10.7	10.7	16	−8.81 to −10.81	+12.95 to +22.77
Aguita									16	−9.86 to +3.45	+16.78 to +21.75
Distal alteration zone											
Bermejal	Qz	18	108 to 217	135	−6.5 to −0.1	−2	0.18 to 10	0.18 to 9.8			
Filos	Qz	15	112 to 120	115	−0.1	−0.1	0.18	0.18			
	Ca	55	103 to 148	119.7	−3.2 to −0.1	−0.7	0.18 to 5.2	1.1			
Nukay	Qz	35	100 to 126	105	−0.2 to −0.1	−0.15	0.265	0.265			
	Ca	21	102 to 165	129	−0.3 to −0.1	−0.15	0.24	0.26			
Unaltered limestone (Morelos formation)											
Nukay									4	+0.53 to +3.17	+19.71 to +22.53
Aguita									4	−0.86 to +3.90	+18.88 to +23.64
Bermejal									5	+1.58 to +2.73	+16.83 to +28.92

blage is end-member diopside whereas the late pyroxene assemblage contains up to 75% hedenbergite. Most garnets are grossularitic, although many are compositionally zoned to andradite. Scapolite and clays occur as fine-grained alteration products in the igneous matrix (Fig. 3a–c). Exoskarn mineralogy is characterized by an assemblage of pyroxene (diopside/hedenbergite; Fig. 4), magnetite, a few coarse-grained euhedral garnet crystals (grossular/andradite, Fig. 4) and, locally, wollastonite (close to the contact between skarn and recrystallized limestone). Antigorite and calcite occur only along the skarn- recrystallized limestone contact.

A retrograde alteration event affects both the endoskarn and exoskarn. It is characterized by an early propylitic alteration mainly consisting tremolite, actinolite, phlogopite, chlorite, epidote, sericite, quartz, and carbonate. The argillic alteration event overprints the former event and is represented by the formation of illite, smectite, kaolinite, carbonate and/or anhydrite.

The economic mineralization consists of lenses and mantos of massive iron oxides (hematite-goethite-magnetite-gold). Gold occurs as native gold or argentine gold with more than 80% of the gold being associated with hematite (Fig. 3b) and jasper-calcite filling late pockets. As a general rule, the gold grade seems to be inversely proportional to the clay argillic alteration intensity. Scarce sulfides (< 1%), mainly pyrrhotite, chalcopyrite, pyrite, marcasite, are common both in inner and outer zones, complete the paragenesis. Arsenopyrite, chalcocite, covellite, bismutite, bornite and molybdenite are specific to the inner mineralizing system, whereas galena and sphalerite are characteristic of the outer mineralized system.

The mineralogy of the Mezcala deposits is similar to the mineralogical succession described for the McCoy oxidized gold skarn type (Brooks et al. 1991; Brooks 1994). As in the Mezcala skarn, the essential features of this type of gold-bearing skarn deposits are the high garnet/pyroxene ratio, a high ferric/ferrous ratio (> 1; De la Garza et al. 1996), predominance of Fe-poor garnet and pyroxene, low total sulfides, and high-temperature brines coupled with a low pressure of formation

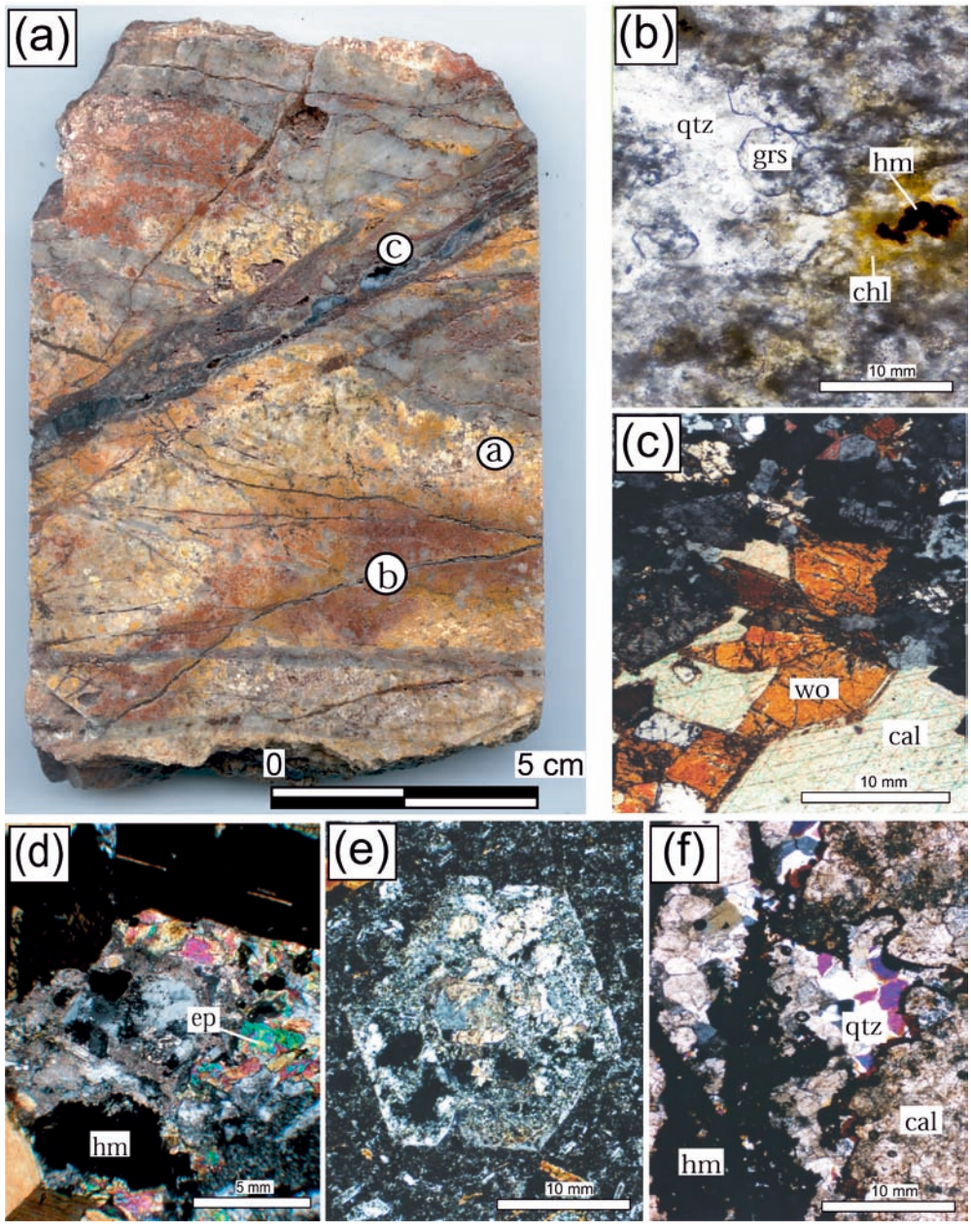

Fig. 3 **a** Photograph of a typical rock alteration succession. *a* Potassic alteration (orthoclase, scapolite, antigorite); *b* Inner alteration zone (tremolite to actinolite, phlogopite, chlorite, epidote, sericite,); *c* Outer alteration zone (Au rich) (illite, smectite, kaolinite, carbonate and/or anhydrite); Agüita intrusive, see Fig. 2. **b** Photomicrograph of inner grossular alteration crosscutting outer zone quartz vein with chlorite and hematite; Nukay south open pit. **c** Photomicrograph of wollastonite-calcite assemblage characteristic of the exoskarn prograde phase (garnet, pyroxene, magnetite, and locally antigorite); Bermejal close to the ore body-intrusive contact. **d** Photomicrograph of an epidote and hematite pocket characteristic of the early propylitic alteration association in the exoskarn zone; Bermejal ore body. **e** Photomicrograph of sericitised porphyritic potassic feldspar, characteristic of the early propylitic alteration association in the endoskarn zone; Bermejal intrusive-ore body contact. **f** Photomicrograph of quartz-calcite-hematite association of the distal outer alteration zone (late retrograde alteration event, and gold richest part); Nukay north open pit, distal ore body extremity. Abbreviations: *cal* calcite; *chl* chlorite; *ep* epidote; *grs* grossular; *hm* hematite; *mr* marcasite; *qtz* quartz; *wo* wollastonite

(ca. 400 bars). In addition, the highest gold grades are not associated with the prograde garnet-pyroxene phase, rather with the retrograde alteration.

U/Pb geochronology constraints

Zircons from the Nukay adakite stock were extracted from the freshest part of a drill-core (30 m deep) and selected for dating the magmatic event that created the Fe-Au-skarn mineralization at Mezcala (Fig. 2). In-situ analyses were carried out at the CRPG-CNRS using a IMS 1270 CAMECA ion-probe of Nancy, France. The analyzed zircons are small (< 200 μm), and prismatic or needle-shaped. SEM analyses reveal regular, fine-scale magmatic zonation and, for some of them an inherited core or a metamict area (Fig. 6; Table 3). Concordia $^{207}Pb/^{235}U$ vs $^{206}Pb/^{238}U$ diagram for zircons is shown in Fig. 6; errors represent analytical precision at 1σ (see Deloule et al. 2002 for a complete description of the analytical procedure).

Twenty-two analyses provided $^{206}Pb/^{238}Pb$ ages dispersed between 59 ± 1 and $1{,}057 \pm 17$ Ma (Fig. 6). Seventeen of the $^{206}Pb/^{238}U$ and $^{207}Pb/^{235}U$ ages are concordant or subconcordant and six are discordant. The highest intrinsic error on $^{207}Pb/^{235}U$ ages and $^{206}Pb/^{238}U$ ages yield elliptical-shaped representative points on the concordia diagram (Fig. 6). Indeed, the $^{207}Pb/^{235}U$ ages are most sensitive to a common lead contribution because the ^{207}Pb ion signal is about ten times lower than the ^{206}Pb ion signal. Additionally the ^{207}Pb, product of the ^{235}U disintegration, present a very

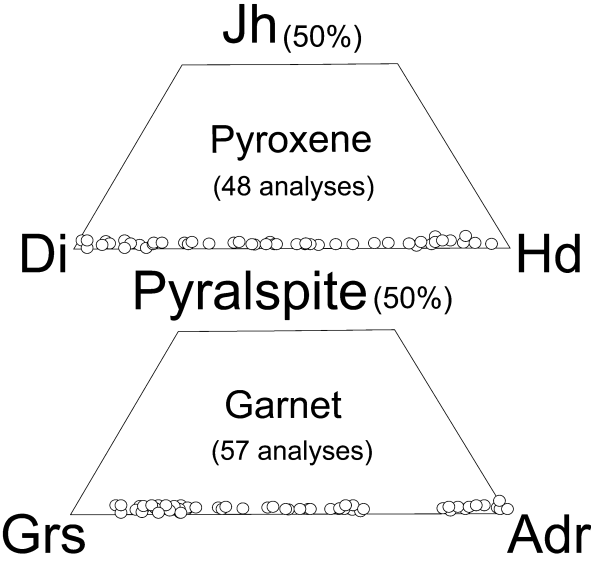

Fig. 4 Ternary plot of (a) Johansonnite (*Jh*)–Diopside (*Di*)–Hedenbergite (*Hd*) pyroxene composition and (b) Grossular (*Grs*)–Andradite (*Adr*)–Pyralspite from the Mezcala skarn

low concentration in young zircon grains. Therefore, the individual $^{206}Pb/^{238}U$ ages appear more reliable for dating purposes. Eight concordant analyses with the youngest ages define a geochronologically homogeneous group (Fig. 6). These yield a weighted mean age of 63 ± 2 Ma, which is interpreted as the emplacement age of the adakite, and consequently the age of the skarn development. This age appears to be in good agreement with the age of the Paleocene magmatism in the Guerrero Terrane event, bracketed from ca. 66 to ca. 41 Ma (Schaaf et al. 1995; Morán-Zenteno et al. 1999). The ten concordant and discordant ages ranging from ca. 78 to 1,057 Ma represent xenocryst grains and inherited cores from plutonic rocks belonging to the Guerrero basement rocks or a mixing-age.

Calcite $\delta^{13}C$ and $\delta^{18}O$ isotopic data

Carbon and oxygen isotopic ratios were measured on CO_2 extracted from calcite and limestone, using the method of McCrea (1950). The isotopic compositions were determined using a Finnigan MAT 250 mass spectrometer of the LUGIS-UNAM, Mexico. Isotope data are reported (Fig. 7) using the delta per mil notation relative to the PDB (carbon) and V-SMOW (oxygen) standards (Craig 1957, 1961). The standard deviation for each analysis is $\pm 0.1‰$ for both carbon and oxygen.

The potential sources for highly oxidizing brines are considered to be the fluids evolved from the adakite stock intrusion and meteoric water circulating through the system and driven by heat from the pluton (González-Partida et al. 2003; Levresse and González-Partida 2003). These alternative sources are evaluated below.

The $\delta^{13}C$ of calcite from apparently unaltered (14 samples) limestones vary from -2.4 to $+3.9‰$; the $\delta^{18}O$ values for these calcites vary from $+16.8$ to $+23.9‰$. The carbon and oxygen isotope compositions of the host rock carbonate are in agreement with the values of comparable Albian-Cenomanian limestones (Huber et al. 1999; Norris et al. 2001; Zürcher et al. 2001). There is no apparent correlation between the isotopic composition of calcite and the stratigraphic position of the sample. The dispersion of the results is supposed to be either related to the organic matter contained in the enclosing rock and/or diagenetic effects.

The depletion of $\delta^{18}O$ and $\delta^{13}C$ in inner alteration zone calcites relative to the fresh limestone is striking (Fig. 7). Inner alteration zone calcites (15 samples) have $\delta^{18}O$ ranging from $+13.2$ to $+14.6‰$, compared to a range from $+16.8$ to $+23.9‰$ for the calcite of the fresh limestone. The $\delta^{13}C$ values of the inner zone calcites are closely grouped, spanning from -11.3 to $-10.0‰$, compared to a range from -2.4 to $+3.9‰$ for the limestone calcite (Fig. 7).

The isotopic compositions of the hydrothermal fluids from which skarn and vein calcite formed can be calculated assuming a formation temperature for calcite saturation, based on fluid inclusion homogenization data. Oxygen isotope fractionation factors between calcite and water were adopted from Kim and O'Neil (1997). For carbon, isotope fractionation factors between CO_2 and calcite were taken from Bottinga et al. (1968). The range of variation of $\delta^{18}O$ ($+13.2$ to $+14.6‰$) and $\delta^{13}C$ (-11.3 to $-10.0‰$) were selected as representative isotope compositions of the inner calcites of the Mezcala deposits (Table 1; Fig. 7). The homogenization temperatures of fluid inclusions in calcite (276 °C) were taken from González-Partida et al. (2003) and Levresse and González-Partida (2003). Consequently, $\delta^{18}O_{SMOW}$ between $+6.8$ and $+8.2‰$ and $\delta^{13}C_{PDB}$ between -8.4 and $-10.5‰$ were calculated for the skarn-forming fluids. According to Zheng and Hoefs (1993), magmatic water may have $\delta^{18}O$ ranging as wide as 6 to $15‰$ with its $\delta^{13}C$ values similar to that the normal mantle (from -9 to $-4‰$). Considering that (1) the calculated isotopic compositions ($\delta^{18}O = 7.3‰$, $\delta^{13}C = -9.2‰$) of the skarn-forming fluids fall within the field of magmatic water, and (2) temperatures (238 to 360 °C) and salinities (> 22.3 equiv. wt% NaCl) were also observed trapped as fluid inclusions at the inner alteration zone (González-Partida et al. 2003; Levresse and González-Partida 2003), it is evident that the hydrothermal fluids involved at the inner alteration zone was a magmatic brine similar to that documented for other skarn systems (Meinert et al. 2003).

Theoretical models for open and closed systems suggested by Zheng and Hoefs (1993) are employed to examine the stable isotope data (Fig. 7). As the amount of magmatic water increased and the skarn evolved, calcite that formed earlier was recrystallized or replaced by new calcite crystals. Therefore, the carbon isotopic composition of the previous crystal might be erased or

Table 2 Analytical results of representative microprobe analyses (wt%) of garnet. pyroxene and wollastonite skarn minerals from the Mezcala Au-skarn deposit. Analytical conditions: current beam 10 nA; accelerated voltage 15 kV

	Mineral Location Protolith	Garnet Core Adakite	Garnet Rim Adakite	Garnet Core Adakite	Garnet Rim Adakite	Garnet Core Limestone	Garnet Core Limestone	Wollastonite Limestone		Pyroxene Ore zone Adakite	Pyroxene Ore zone Adakite	Pyroxene Ore zone Adakite	Pyroxene Ore zone Adakite	Pyroxene Marble limestone
SiO_2		37.53	36.88	36.69	35.08	34.14	35.28	50.71	SiO_2	54.74	53.40	52.69	51.16	49.58
TiO_2		0.51	0.17	0.29	1.39	0.01	0.04	0.00	TiO_2	0.20	0.03	0.04	0.02	0.04
Al_2O_3		19.36	16.50	14.58	7.80	3.56	0.18	0.05	Al_2O_3	0.58	0.03	0.33	0.18	0.07
Fe_2O_3calc.		3.29	7.67	10.19	19.04	26.08	30.98	3.86	Fe_2O3 calc.	0.31	5.83	11.96	17.44	23.75
MnO		0.44	0.31	0.40	0.16	0.04	0.25	0.36	MnO	0.29	0.72	0.90	0.57	1.1
MgO		0.11	0.06	0.04	0.07	0.13	0.03	0.52	MgO	17.54	13.86	10.16	6.85	2.04
CaO		37.89	37.32	36.91	36.06	35.12	33.96	43.67	CaO	25.59	25.45	24.32	23.63	23.36
Na_2O		0.00	0.00	0.00	0.00	0.00	0.00	0.02	Na_2O	0.30	0.05	0.11	0.09	0.02
K_2O		0.00	0.00	0.00	0.00	0.00	0.00	0.02	K_2O	0.00	0.00	0.00	0.03	0.03
Total		99.1	98.8	99.1	99.6	99.1	100.7	99.2	Total	99.4	99.4	100.5	100.0	99.99
Si		2.913	2.912	2.918	2.890	2.890	2.837	0.996	Si	1.991	1.992	2.000	2.000	2.006
Ti		0.019	0.007	0.011	0.056	0.000	0.002	0.000	Ti	0.000	0.001	0.001	0.002	0.000
Al		1.771	1.535	1.367	0.757	0.355	0.019	0.001	Al	0.025	0.001	0.015	0.010	0.003
Fe		0.192	0.450	0.610	1.180	1.661	2.049	0.066	Fe	0.009	0.182	0.380	0.571	0.733
Mn		0.029	0.021	0.027	0.011	0.003	0.019	0.005	Mn	0.009	0.040	0.029	0.018	0.038
Mg		0.013	0.007	0.005	0.009	0.016	0.004	0.019	Mg	0.951	0.771	0.575	0.398	0.128
Ca		3.150	3.157	3.145	3.183	3.176	3.198	0.940	Ca	0.997	1.017	0.989	0.993	1.012
Na		0.000	0.000	0.000	0.000	0.000	0.000	0.001	Na	0.021	0.004	0.008	0.008	0.002
K		0.000	0.000	0.000	0.000	0.000	0.000	0.001	K	0.000	0.000	0.000	0.001	0.002
Total		8	8	8	8	8	8	2	Total	4	4	4	4	4
Cations based on 12 oxygens (mole percent)									Cations based on 6 oxygens (mole percent)					
Pyralspite		1.3	0.9	1.0	0.6	0.6	1.1		Johannsenite	0.9	4.0	2.9	1.8	4.2
Andradite		14.1	23.6	32.0	62.7	87.1	99.8		Diopside	98.1	78.0	58.4	40.3	14.2
Grossular		84.6	75.5	67.0	36.7	12.3	0.0		Hedenbergite	0.9	18.0	38.6	57.9	81.5

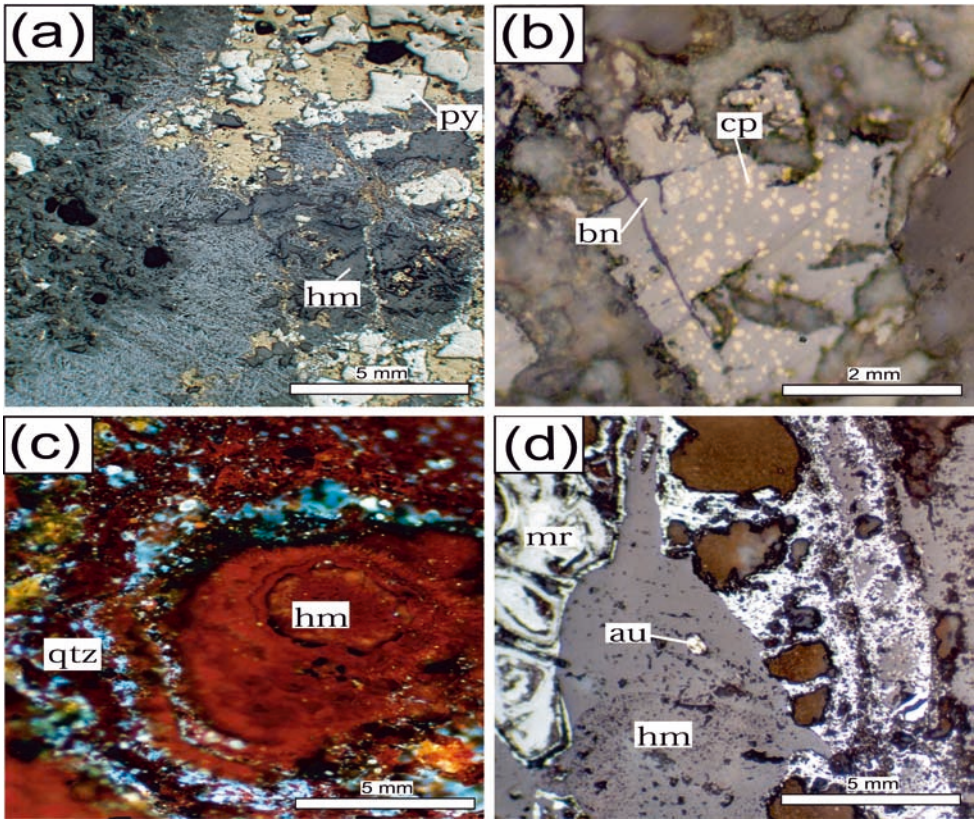

Fig. 5 **a** Photomicrograph of pyrite-hematite-Fe oxide mineralization association in the inner alteration zone; close to the ore body-intrusive contact, Agüita mine Fig. 2. **b** Photomicrograph of sulfide (bornite with chalcopyrite exolution) association in the inner alteration zone; Bermejal open pit. **c** Photomicrograph of hematite and quartz pocket association in the distal outer alteration zone; distal limit of the Nukay principal ore body. **d** Photomicrograph of gold association in the outer alteration zone; Nukay principal ore body. Abbreviations: *au* gold; *bn* bornite; *cp* chalcopyrite; *hm* hematite; *mr* marcasite; *qtz* quartz

homogenized. This recrystallization and replacement also explain why there are no data available for water/rock (volume) ratio between 2 and 20 (Fig. 7). The magmatic water would have dissolved calcite at the fluid dominant (water/rock ratio > 20) environment in the inner zone. Contrasting, the change of the carbon isotopic composition in calcite, as water/rock ratio increases, the oxygen isotope composition of the inner calcite did not change despite the variation of temperature ranging from 350 to 250 °C (Fig. 6). This temperature range is also supported by the homogenization temperatures recorded in calcite (238 to 370 °C, see Table 1). The composition of oxygen is probably buffered by the sedimentary host rock. The CO_2 mole fraction [$X(CO_2)$], was estimated at 0.1 of the carbon and oxygen covariations as shown Fig. 7. This low CO_2 mole fraction is consistent with the fluid inclusion study showing no CO_2 phase observed in the fluid inclusions (González-Partida et al. 2003; Levresse and González-Partida 2003).

The $\delta^{18}O$ and $\delta^{13}C$ composition of the outer calcite zone spans from 13.0 to 22.7‰ and from −11.3 to 3.5‰, respectively. The heterogeneous distribution of the outer $\delta^{13}C$ values is related to the distance from the intrusion and position in the paragenetic succession of the samples. The $\delta^{18}O$ comparable values of the limestone and outer zone support: (1) degassing reactions during the ductile/brittle transition, (2) a strong dilution of the magmatic brine with meteoric fluids (cf. González-Partida et al. 2003; Levresse and González-Partida 2003).

A decrease in geostatic pressure to hydrostatic in the brittle domain may cause a release of $CO_{2(g)}$ causing an increase in pH and triggering the precipitation of carbonates. As $CO_{2(g)}$ evolution tends to fractionate the heavier carbon isotope (Bowers 1991), the fluid would be progressively depleted in ^{13}C, as recorded in calcite. The decreasing salinity is explained by meteoric water incursion along existing fracture network. The cooling and the mixing of a fluid in isotopic equilibrium with the adakite stock with a meteoric fluid in isotopic equilibrium with the limestone would result in the change of the oxygen isotopic composition of the calcite to higher values. The comparable oxygen mean values of the outer alteration calcite (from +13.0 to +22.7‰) and the fresh limestone (from +16.8 to +28.9‰), and the wide range of carbon isotope variation of the outer alteration zone calcite (−11.3 to 3.5‰) are best interpreted as the degassing of a magmatic brine, in isotopic equilibrium with the adakite stock, and its dilution with a meteoric fluid which is in turn in isotopic equilibrium with a reservoir within the Cretaceous limestones.

Precipitation mechanisms

Generally, the transport and precipitation of Au in oxidized porphyry and the oxidized Au-rich skarn environments is favored by dense, oxidizing magmatic brines (T≈400 to 700 °C; salinity≈40 to 70 wt% NaCl eq.) that have undergone boiling and/or strong dilution with meteoric waters (Henley and McNabb 1978; Sillitoe

Table 3 U/Pb isotopic data for single zircon crystal from Nukay adakite obtained by ion microprobe analysis (CAMECA IMS 1270)

Label	Measured data					Content			Concordia inverse				Concordia					Ages U-Pb			
	Is	^{206}Pb	$^{207}Pb/^{206}Pb$	$^{204}Pb/^{206}Pb$	$^{206}Pb/^{238}U$	UO/U	Pb (ppm)	U (ppm)	Th (ppm)	$^{238}U/^{206}Pb$	±	$^{207}Pb/^{206}Pb$	±	$^{207}Pb/^{235}U$	Error	$^{206}Pb/^{238}U$	Error	Correl. err	$^{206}Pb/^{238}U$	Error	$^{207}Pb/^{235}U$	Error
mx1	1,928	0.04921	0.00047	0.022	7.73	0.8	99.4	47.3	109.26	1.92	0.049	0.000	0.060	0.001	0.009	0.000	0.770	59	1	60	1
mxx7	3,323	0.04906	0.00010	0.024	7.01	6.4	775.8	232.2	104.92	1.00	0.049	0.000	0.063	0.001	0.010	0.000	0.783	61	1	62	1
mxx10	2,248	0.04780	0.00013	0.024	7.01	3.1	377.8	112.8	104.18	1.17	0.048	0.000	0.061	0.001	0.010	0.000	0.941	62	1	60	1
mx17	1,691	0.04844	0.00038	0.014	6.15	0.5	55.8	22.5	103.22	2.05	0.048	0.001	0.066	0.002	0.010	0.000	0.766	62	1	65	2
mx15	1,272	0.04890	0.00057	0.015	6.30	0.4	45.8	13.7	103.08	2.53	0.049	0.000	0.066	0.002	0.010	0.000	0.696	62	2	64	2
mx13	1,375	0.04732	0.00034	0.018	6.72	0.5	64.1	25.4	101.32	1.94	0.047	0.000	0.068	0.002	0.010	0.000	0.811	63	1	67	2
mxx1	2,659	0.04821	0.00010	0.025	7.01	4.6	526.3	213.1	97.95	0.95	0.048	0.000	0.066	0.001	0.010	0.000	0.792	65	1	65	1
mx6	2,206	0.04711	0.00021	0.027	8.10	1.9	211.9	84.4	96.75	1.60	0.047	0.000	0.070	0.001	0.010	0.000	0.811	66	1	68	1
mxx8	4,211.3	0.05337	0.00041	0.028	6.81	7.9	761.5	316.0	82.49	2.56	0.053	0.001	0.079	0.003	0.012	0.000	0.839	78	2	77	3
mxx4	10,320	0.04872	0.00003	0.056	7.37	15.1	826.3	472.5	47.13	0.44	0.049	0.000	0.142	0.001	0.021	0.000	0.911	135	1	134	1
mxx4	9,460	0.04892	0.00003	0.056	7.32	15.1	821.4	457.2	46.73	0.44	0.049	0.000	0.143	0.001	0.021	0.000	0.894	136	1	136	1
mxx2	3,893	0.05643	0.00011	0.084	7.52	6.5	246.8	52.4	32.50	1.37	0.056	0.000	0.233	0.010	0.031	0.001	0.983	195	8	213	8
mx16	2,251	0.05195	0.00035	0.046	5.68	0.8	24.6	10.6	26.15	1.39	0.052	0.000	0.272	0.015	0.038	0.002	0.957	242	13	244	12
mxx6	7,440	0.07316	0.00003	0.427	7.20	10.4	72.9	33.0	6.02	0.06	0.073	0.000	1.668	0.016	0.166	0.002	0.968	990	8	996	6
mx11	20,096	0.07845	0.00003	0.338	6.90	6.7	44.9	13.5	5.73	0.21	0.078	0.000	1.893	0.070	0.175	0.006	0.999	1,037	35	1,078	24
mx5	15,202	0.07808	0.00010	0.508	8.43	4.7	30.7	10.0	5.61	0.10	0.078	0.000	1.900	0.033	0.178	0.003	0.983	1,057	17	1,081	12
mx10	840	0.04885	0.00040	0.027	7.96	0.5	61.2	40.4	96.03	1.97	0.049	0.000	0.080	0.003	0.010	0.000	0.656	67	1	78	2
mx3	1,325	0.04883	0.00019	0.031	8.49	0.9	98.6	47.6	92.32	1.47	0.049	0.000	0.081	0.002	0.011	0.000	0.755	69	1	79	2
mx9	779	0.04910	0.00044	0.033	8.67	0.6	59.4	19.3	89.37	1.60	0.049	0.000	0.087	0.002	0.011	0.000	0.666	72	1	85	2
mx7	390	0.05120	0.00027	0.031	8.27	0.3	27.5	7.2	85.89	1.56	0.051	0.000	0.119	0.003	0.012	0.000	0.650	75	1	114	3
mxx9	10,892	0.07196	0.00003	0.177	7.13	18.7	312.5	126.8	14.35	0.76	0.072	0.000	0.689	0.037	0.070	0.004	0.998	434	22	532	22
mxx5	9,111	0.06320	0.00010	0.254	8.11	20.2	282.9	84.2	12.00	0.15	0.063	0.000	0.710	0.010	0.083	0.001	0.915	516	6	545	6

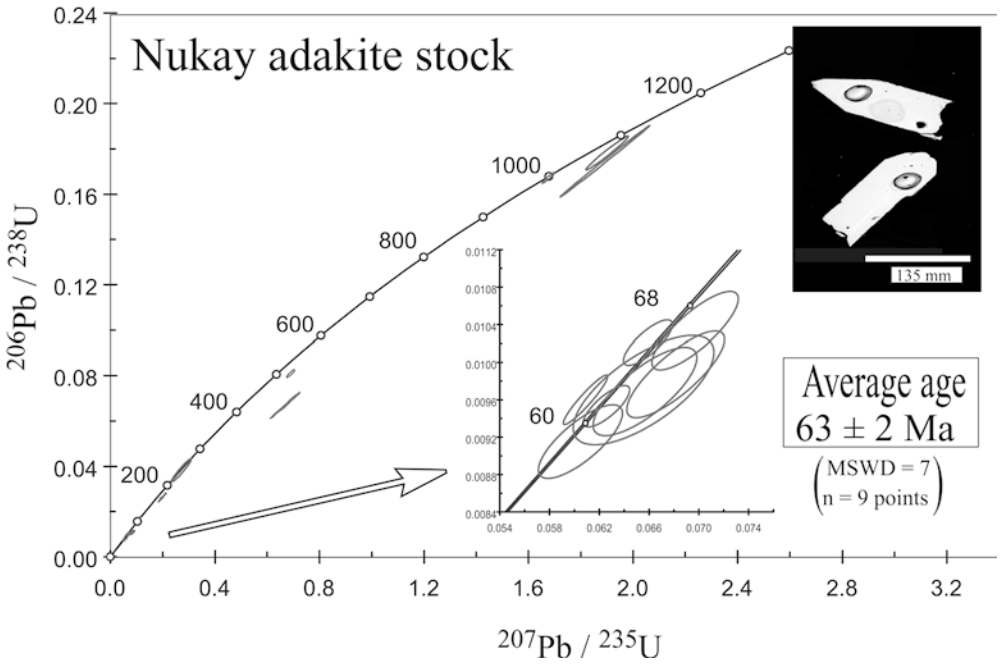

Fig. 6 $^{206}Pb/^{238}U$ versus $^{207}Pb/^{235}U$ plot of zircon ion microprobe analyses (CAMECA IMS 1270) for the Nukay adakite. Ages are calculated with the Isoplot program (Ludwig 2000). The elliptic holes on the grains of SEM images (*insets*) are examples of spot positions in the analyzed zircon grains

1988; Gammons and Williams-Jones 1997; Meinert 1995; Muntean and Einaudi 2000). Gold transport in oxidized environments is complex as thermodynamic calculations indicated a switchover from a chloride complex to a more soluble bisulfide complex with cooling of the ore fluids (Gammons and Williams-Jones 1997). The temperature of the chloride-bisulfide transition, typically ranging from 350 to 450 °C, depends on the pH and the H_2S/Cl ratio of the original fluid and whether or not immiscibility occurs. In an oxidized magma, the sulfur species concentration is $SO_2 > > H_2S$, which implies a ΣS^{2-} relatively low in general. The change of the transporting ligand for Au reasonably explains the distal position of the Au-rich zones in a classic oxidized porphyry and/or skarn deposit. These processes are evidenced by the fluid composition and the isotopic evolution we found in the Mezcala district.

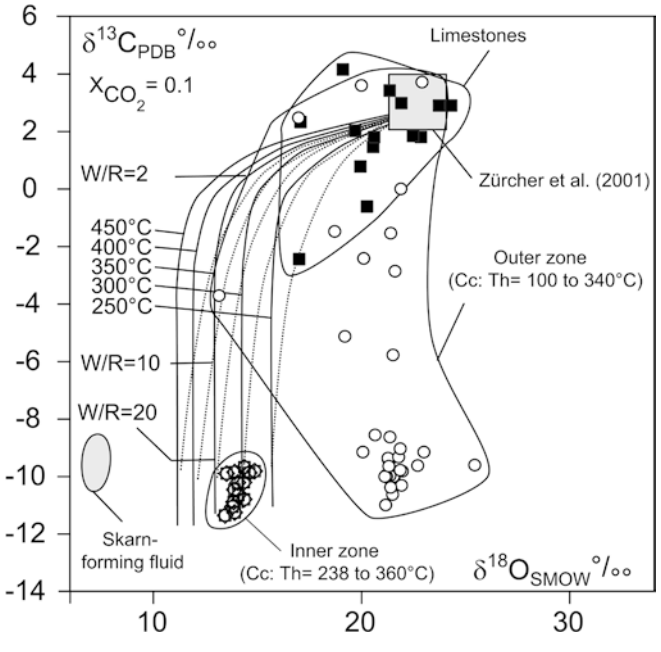

Fig. 7 Plot of $\delta^{18}O$ vs. $\delta^{13}C$ analytical values for calcite in the Mezcala area. Symbols are: calcite from inner alteration zone (*open star*); calcite from outer alteration zone (*open circle*); unaltered limestone (Morelos Formation; *black square*). Abbreviations: *Cc* calcite; *Th* homogenization temperature; *W*/*R* water/rock ratio

Magmatic gold is usually transported as chloride complexes, while precipitation occurs due to a decrease in Cl^- concentration and/or an increase in pH. Dilution of a magmatic birne is the most effective way of decreasing ΣCl by mixing with convective waters of non-magmatic origin (Gammons and Williams-Jones 1997). Also, an increase in the pH of the solution could also be related to the water-carbonate rock interaction (Gammons and Williams-Jones 1997). Boiling is a critical process in hydrothermal environment, as boiling and the subsequent gas loss is the cause of primary orthomagmatic fluid basification, since the most acidic components (HCl, H_2S, SO_2) are known to fractionate into the vapor phase relative to their basic counterparts (KCl, NaCl, HS^-). Generally, boiling induces gold precipitation from bisulfide complexes, as gold saturation occurs due to the loss of the sulfide ligand to the vapor phase. Boiling also causes cooling and concentration of dissolved species such as silica, lending to quartz supersaturation and the formation of silica colloids. The lack of sulfides in the Mezcala mineralizations suggests H_2S degassing and very high $f\ O_2$ during the mineralizing process. The significant gold deposition in the outer alteration zone implies that the Mezcala magmatic oxidized brine had the appropriate f O2, pH and ΣCl

conditions that allowed the transport of gold as $AuCl^-$ or $AuCl_3$ complexes at relatively low temperatures. According to the fluid inclusions and stable isotopes results, we conclude that the temperature of the ductile/brittle transition, intimately related with the meteoric fluid invasion of the system, is probably a key to understanding the precipitation mechanism in a pH increasing, dilution and cooling context.

Conclusions

The mineralogical characteristics of the Fe-Au Mezcala skarn deposits are: (1) the high garnet/pyroxene ratios, (2) a high ferric/ferrous ratios, (3) Fe-poor garnet and pyroxene, (4) low total sulfides, (5) the presence of a high-temperature brine, (6) a low pressure of formation and (7) the highest gold grade associated with the outer alteration. All these characteristics lead to classify the Mezcala deposits as an oxidized Fe-Au skarn type.

The results of U/Pb dating on zircon constrain both the age of the emplacement of the Mezcala adakite stock (63 ± 2 Ma) and, indirectly, the hydrothermal alteration related system.

The magmatic origin of the fluids and the evolutionary history of the Fe-Au Mezcala skarn deposits were also revealed from the carbon and oxygen isotope covariations of the inner calcite zone. In the outer zone, the mixing of the degassed gold-rich magmatic brines with meteoric water may be responsible for boiling, dilution, and cooling of the resulting solution, processes that could cause the deposition of gold.

Acknowledgements The Peñoles Mining Corporation is thanked for logistical field assistance and for the permission to publish the results. This study was funded in part by scientific grants UNAM-PAPIIT (# IN100900), CONACYT (# G35442-T) to E. González-Partida and CRPG-UPR2300A to A. Cheilletz and D. Gasquet. Dave Lentz and Laurence Meinert are thanked for their constructive observations and careful English changes that significantly improved the manuscript. Zircon ion-probe analysis were carried out under the supervision of E. Deloule, M. Champenois and D. Mangin.

References

Bottinga Y (1968) Calculation of fractionation factors for carbon and oxygen exchange in the system calcite–carbon dioxide–water. J Phys Chem 72:800–808

Bowers TS (1991) The deposition of gold and other metals: pressure-induced fluids immiscibility and associated stable isotope signature. Geochim Cosmochim Acta 55:2417–2434

Brooks W (1994) Petrology and geochemistry of the McCoy gold skarn, Lander County, Nevada. PhD Thesis, Washington State University, Pullman, Washington, USA, 607 pp

Brooks JW, Meinert LD, Kuyper BA, Lane ML (1991) Petrology and geochemistry of the McCoy gold skarn, Lander County, NV. In: Raines GL, Lisle RE, Schafer RW, Wilkinson WH (eds) Geology and ore deposits of the Great Basin. Geol Soc Nevada, Reno 1:419–442

Burnham CW (1997) Magmas and hydrothermal fluids. In: Barnes HL (ed) Geochemistry of hydrothermal ore deposits, 3rd edn. Wiley, New York, p 63–118

Clark KF, Foster CT, Damon EP (1982) Cenozoic mineral deposits and subduction-related magmatic arcs in Mexico. Geol Soc Am Bull 93:533–544

Craig H (1957) Isotopic standards for carbon and oxygen and correction factors for mass spectrometry analysis of carbon dioxide. Geochim Cosmochim Acta 12:133–149

Craig H (1961) Standards for reporting concentrations of deuterium and oxygen-18 in natural waters. Science 133:1833–1834

De la Garza V, Téllez R, Díaz R, Hernández A (1996) Geology of the Bermejal iron-gold deposit Mezcala, Guerrero, México. In: Coyner AR, Fahey PL (eds) Geology and ore deposits of the American Cordillera. Geol Soc Nevada Symp Proc, Reno/Sparks, Nevada, April 1995. 111:1354–1368

Defant MJ, Drummond MS (1990) Derivation of some modern arc magmas by melting of young subducted lithosphere. Nature 347:662–665

Deloule E, Alexandrov P, Cheilletz A, Laumonier B, Barbey P (2002) In situ U/Pb zircon ages for Early Ordovician magmatism in the eastern Pyrenees, France: the Canigou orthogneisses. Int J Earth Sci 91:398–405

Fríes C (1960) Geología del Estado de Morelos y de partes adyacentes de México y Guerrero, región central meridional de México. Instituto de Geología, Boletín 60, 236 pp

Gammons CH, Williams-Jones AE (1997) Chemical mobility of gold in the porphyry-epithermal environment: Econ Geol 92:45–59

González-Partida E, Levresse G, Cheilletz A, Gasquet D, Jones D (2003) Paleocene adakite bearing Fe-Au intrusive rocks, Mezcala, Mexico: evidence from geochemical characteristics. J Geochem Explor 4105:1–16

González-Partida E, Torres-Rodríguez V (1988) Evolución tectónica de la porción centro-occidental de México y su relación con los yacimientos minerales asociados. Geofis Int 27:543–581

Hedenquist JW (1987) Mineralization associated with volcanic-related hydrothermal systems in the Circum-Pacific basin. In: Horn MK (ed) Circum-Pacific Energy and Mineral Resources Conference, 4 th, Singapore 1986, Trans. Tulsa, Oklahoma. Am Assoc Petrol Geology, pp 513–524

Henley RW, McNabb A (1978) Magmatic vapor plumes and ground-water interaction in porphyry copper emplacement: Econ Geol 73:1–20

Huber BT, Leckie RM, Norris RD, Bralower TJ, CoBabe E (1999) Foraminiferal assemblage and stable isotopic change across the Cenomanian Turonian boundary in the subtropical Atlantic. J Foramin Res 29:392–417

Jones D, González-Partida E (2001) Evidence of magmatic fluid flux and "recapture" in mineralizing granodiorites of the Nukay Au (-Cu) skarn district, Gro. Mexico. Mexico XXIII convention Nacional AIMMGM, AC, Mexico

Jones D, Jackson PR (2001) Geology and mineralization of Los Filos gold deposit, Nukay district, Guerrerro, Mexico. Mexico XXIII convention Nacional AIMMGM, AC, Mexico

Kim ST, O'Neil JR (1997) Equilibrium and nonequilibrium oxygen isotope effects in synthetic carbonates. Geochim Cosmochim Acta 61:3461–3475

Levresse G, González-Partida E (2003) High oxidised gold skarn fluids analysis in the Mezcala deposit, Gro., Mexico. J Geochem Explor 78–79:649–652

Ludwig KR (2000) Isoplot/Ex 2.49. A geochronological toolkit for Microsoft Excel. Berkeley Geochronolgical Center Spec Publ N°1a, 58 pp

Maury RC, Sajona FG, Pubellier M, Bellon H, Defant MJ (1996) Fusion de la croute oceanique dans les zones de subduction/collision recentes: L'exemple de Mindanao (Philipinas): Bull Soc Geol Fr 167:579–590

McCrea JM (1950) On the isotopic of carbonates and paleotemperature scale. J Chem Phys 18:849–857

Meinert LD (1992) Skarns and skarn deposits. Geosci Can 19:145–162

Meinert LD (1995) Compositional variation of igneous rock associated with skarns deposits-chemical evidence for a genetic connection between petrogenesis and mineralization. In: Thompson

JFH (ed) Magma, fluids and ore deposits. Mineral Assoc Can, Short Course 23:401–418

Meinert LD, Hedenquist JW, Satoh H, Matsuhisa Y (2003) Formation of anhydrous and hydrous skarn in Cu-Au-ore deposits by magmatic fluids. Econ Geol 98:147–156

Meinert LD, Hefton KK, Mayes D, Tasiran I (1997) Geology, zonation, and fluid evolution of the Big Gossan Cu-Au skarn deposit, Ertsberg district, Irian Jaya. Econ Geol 92:509–534

Morán-Zenteno DJ, Tolson G, Martínez-Serrano R, Martiny B, Schaaf P, Silva-Romo G, Macías-Romo C, Alba-Aldave L, Hernández-Bernal MS, Solis-Pichardo GN (1999) Tertiary arc-magmatism of the Sierra Madre del Sur, México, and its transition to the volcanic activity of the Trans-Mexican Volcanic Belt. J South Am Earth Sci 12:513–535

Muntean JL, Einaudi MT (2000) Porphyry gold deposits of the Refugio District, Maricunga Belt, northern Chile. Econ Geol 95:1445–1472

Norris RD, Kroon D, Huber BT, Erbacher J (2001) Cretaceous Palaeogene ocean and climate change in the subtropical North Atlantic. In: Kroon D, Norris RD, Klaus A (eds) Western North Atlantic Palaeogene and Cretaceous palaeoceanography. Geol Soc Lond Spec Publ 183:1–22

Schaaf P, Morán-Zenteno D, Hernández-Bernal M (1995) Paleogene continental margin truncation in southwestern Mexico: geochronological evidence. Tectonics 14:1339–1350

Sillitoe RH (1988) Gold deposits in western Pacific island arcs: the magmatic connection. Econ Geol Monogr 6:274–291

Tritlla J, Camprubí A, Centeno E, Corona-Esquivel R, Iriondo A, Sánchez-Martínez S, Gasca-Durán AA, Cienfuegos-Alvarado E, Morales-Puente P (2003) Estructura y edad del depósito de Fe de Peña Colorado (Colima): un posible equivalente Fanerozoico de los depósitos de tipo IOCG. Revista

Zheng YF, Hoefs J (1993) Carbon and oxygen isotope covariations in hydrothermal calcites: theoretical modeling on mixing processes and application to kushikino gold mining area in Japan. Mineral Deposita 25:246–250

Zürcher L, Ruiz J, Barton MD (2001) Paragenesis, elemental distribution, and stable isotopes at the Peña Colorda iron skarn, Colima, Mexico. Econ Geol 96:535–557